The scaling relationship between self-potential and fluid flow on Masaya volcano, Nicaragua

J. L. Lewicki
Earth Sciences Division, Lawrence Berkeley National Laboratory, Berkeley, CA, USA
G. E. Hilley
Department of Earth and Planetary Sciences, University of California, Berkeley, CA, USA.
C. Connor
Department of Geology, University of South Florida, Tampa, FL, USA

ABSTRACT: The concurrent measurement of self-potential (SP) and soil CO_2 flux (F_s^{CO2}) in volcanic systems may be an important tool to monitor intrusive activity and understand interaction between magmatic and groundwater systems. However, quantitative relationships between these parameters must be established to apply them toward understanding processes operating at depth. Power-law scaling exponents calculated for SP and F_s^{CO2} measured along a fault on the flanks of Masaya volcano, Nicaragua indicate a nonlinear relationship between these parameters. Scaling exponents suggest that there is a declining increase in SP with a given increase in F_s^{CO2}, until a threshold (log $F_s^{CO2} \approx 2.5\ g\ m^{-2}d^{-1}$) above which SP remains constant with increasing F_s^{CO2}. Implications for subsurface processes that may influence SP at Masaya are discussed.

1 INTRODUCTION

SP anomalies have been observed within many volcanic and hydrothermal regions, and SP variations have been linked to changes in volcanic activity and hydrothermal fluid flow (Corwin and Hoover 1979; Fitterman and Corwin 1982; Massenet and Pham 1985; Hashimoto and Tanaka 1995; Zlotnicki et al. 2003). Monitoring these anomalies on active volcanoes may therefore be a tool to forecast eruptions and understand interaction between magmatic and groundwater systems. SP anomalies observed in volcanic systems have been primarily attributed to electrokinetic (EK) processes involving transport of charge contained in the electrical diffuse layer at the pore surface by electrolyte solution flow (Anderson and Johnson 1976; Massenet and Pham 1985; Revil et al. 1999; Ishido and Pritchett 1999) or rapid fluid disruption (RFD), a process whereby charge separation can be produced by rapid disruption or vaporization of liquid water by high heat and/or gas flow (Johnston et al. 2001). While EK potentials are produced by capillary flow of aqueous solutions, RFD may produce positive SP anomalies in thermal areas far above the groundwater table as charge is carried by water droplet and/or vapor flow (Johnston et al. 2001).

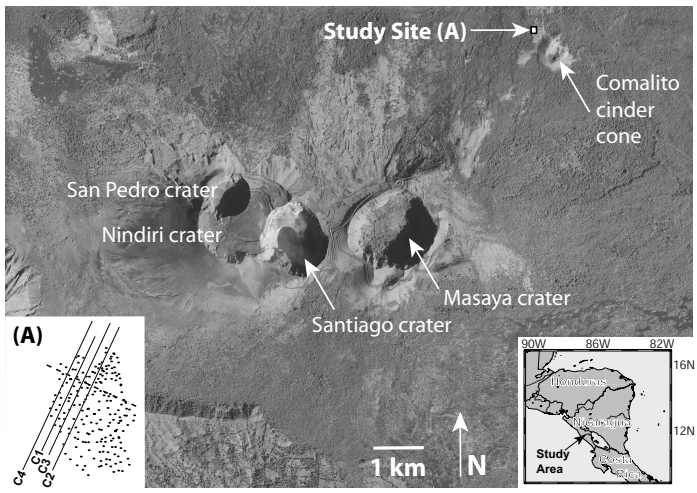

Figure 1: Areal photograph showing study site location adjacent to Comalito cinder cone on the flanks of Masaya volcano. Inset (A) shows locations of SP and F_s^{CO2} transects C1-C4, areal F_s^{CO2} measurements (dots), and inferred normal fault (dashed line).

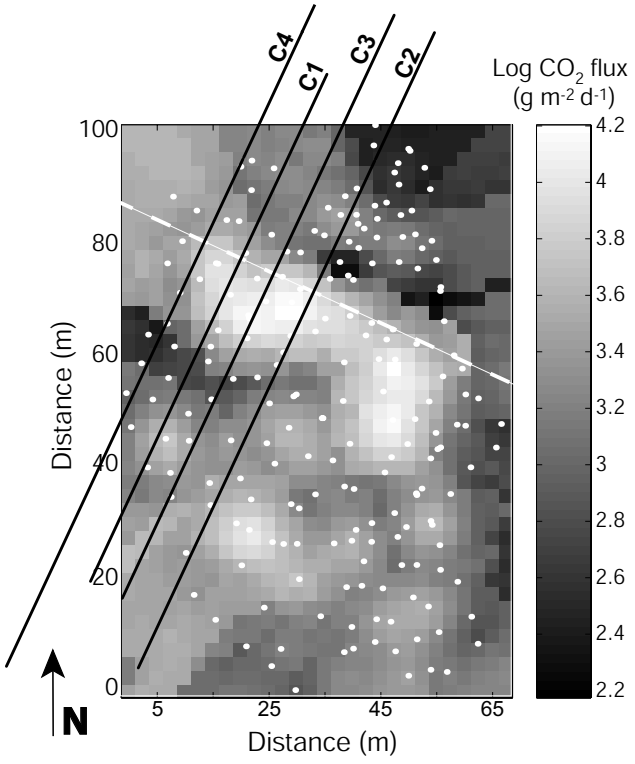

Figure 2: Interpolated image map of log F_s^{CO2} measured adjacent to Comalito cinder cone (Lewicki et al. 2003). Dashed line and dots show locations of inferred normal fault and F_s^{CO2} measurements, respectively. Also shown are locations of transects C1-C4.

Lewicki et al. 2003 investigated the spatial relationship between SP, F_s^{CO2}, and soil temperature (T_s) and the mechanism(s) that may produce SP anomalies on the flanks of Masaya volcano, Nicaragua (Figure 1). F_s^{CO2} and T_s up to 5.0 x 10^4 g $m^{-2}d^{-1}$ and 80^{o}C, respectively, and positive SP anomalies were measured within an area surrounding an inferred normal fault, adjacent to Comalito cinder cone (Figure 2). Lewicki et al. 2003 showed that SP, F_s^{CO2}, and T_s were spatially correlated and that trends in F_s^{CO2} and T_s were consistent with advective transport of heat and CO_2 with steam along a fault zone. Also, a model calculation (Babu 2003) showed that polarization must be shallow ($<$10 m) to produce the high horizontal SP gradients and short wave lengths observed at the study site. Based on the presence of mechanisms to produce RFD (i.e., subsurface temperatures above liquid boiling points, high gas flow rates), a thick unsaturated zone (100 to 150 m), and relatively high resistivities, Lewicki et al. 2003 suggested that SP anomalies at Masaya are mainly produced by RFD.

While clear spatial correlation was observed between SP and F_s^{CO2}, Lewicki et al. 2003 did not investigate the quantitative relationship between these parameters. Such a link is important to establish to better understand the influence of fluid flow processes operating at depth on SP anomalies measured at the surface. Here, we establish power-law scaling relationships for measured values and discuss the subsurface processes that may influence SP at Masaya.

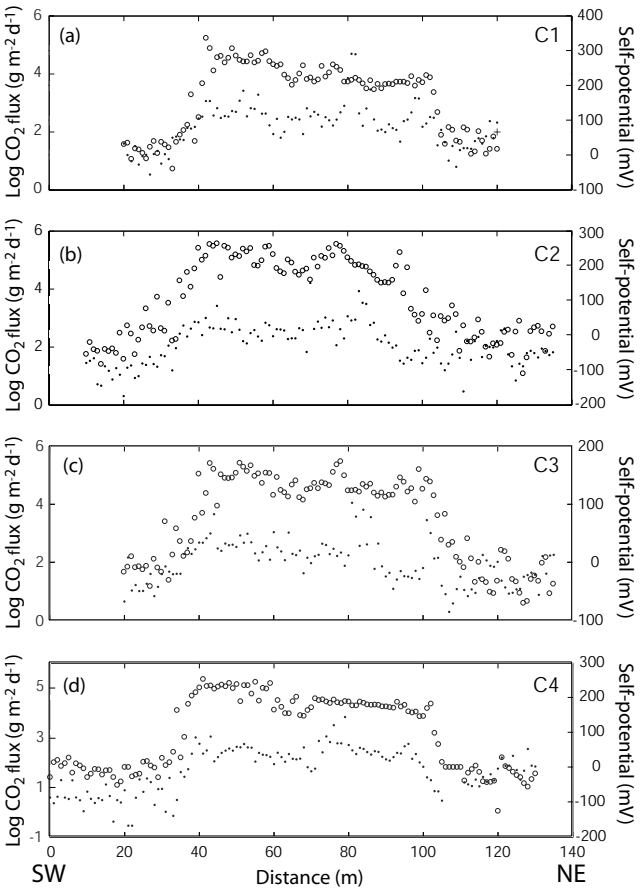

Figure 3: Plots of log F_s^{CO2} (dots) and SP (open circles) versus distance along transects (a) C1, (b) C2, (c) C3, and (d) C4 (modified from Lewicki et al. 2003).

2 DATA ANALYSIS

Scaling relationships between SP and F_s^{CO2} were calculated by linear regression of the log-transformed data. These relationships were determined separately for each traverse (C1-C4) because SP measurements along each traverse were referenced to the background base station at the southwest end of each traverse (Lewicki et al. 2003). To remove background effects not attributable to processes within the fault zone, we subtracted F_s^{CO2} measured at each background base station from all measurements along each traverse. These values are reported as "adjusted" F_s^{CO2}. Since SP represents the electric potential difference between the base station and a given measurement along the traverse, adjustment was unnecessary.

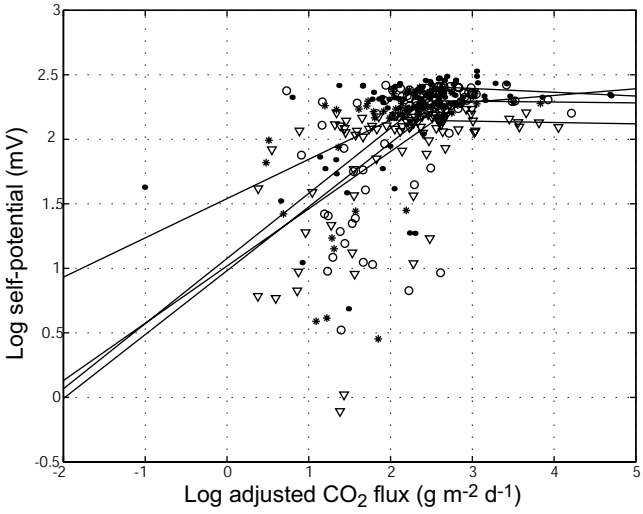

Figure 4: Plot of log SP versus log adjusted F_s^{CO2} for transects C1 (dots), C2 (circles), C3 (triangles) and C4 (stars). Best-fit lines determined by linear regression are shown for log adjusted $F_s^{CO2} \leq 2.5$ g m^{-2}d^{-1} and log adjusted $F_s^{CO2} > 2.5$ g m^{-2}d^{-1}.

Table 1: Parameters a and b calculated for best-fit lines to log SP versus log adjusted F_s^{CO2}, log SP versus log adjusted T_s, and log adjusted T_s versus log adjusted F_s^{CO2}. The mean (μ) and standard error (σ) of a and b are shown.

	$SP = b(F_s^{CO2})^a$			
traverse	log $F_s^{CO2} \leq 2.5$		log $F_s^{CO2} > 2.5$	
	a	b	a	b
C1	0.30	1.5	-2.9e^{-2}	2.5
C2	0.50	0.98	5.2e^{-2}	2.1
C3	0.44	1.0	-1.0e^{-2}	2.2
C4	0.50	1.1	-6.8e^{-3}	2.3
μ	0.44	1.2	1.4e^{-3}	2.3
σ	9.2e^{-2}	0.26	3.5e^{-2}	0.16

3 RESULTS

Self-potential and log F_s^{CO2} measured along transects C1-C4 (Figure 3) are moderately positively correlated (correlation coefficient, C = 0.67, 0.71, 0.59, and 0.70 for transects C1, C2, C3, and C4, respectively). A plot of log SP versus log adjusted F_s^{CO2} for transects C1-C4 (Figure 4) shows a sharp change in correlation of these parameters at log $F_s^{CO2} \approx 2.5$ g m^{-2}d^{-1}. Log SP and log adjusted F_s^{CO2} are moderately positively correlated (C = 0.44 to 0.56 for C1-C4) at log $F_s^{CO2} \leq 2.5$ g m^{-2}d^{-1} and poorly correlated (C = -0.25 to 0.08 for C1-C4) at log $F_s^{CO2} > 2.5$ g m^{-2}d^{-1}.

Linear regression of log-transformed values of SP and adjusted F_s^{CO2} was used to calculate the power-law scaling for SP versus adjusted F_s^{CO2}:

$$SP = b(F_s^{CO2})^a \quad (1)$$

(Figure 4). In the log-transformed space, the regressed slope yields the exponent value (a) and the intercept yields the scaling constant (b). Table 1 shows calculated power-law coefficients for transects C1-C4.

4 DISCUSSION AND CONCLUSIONS

We assume that rapid disruption (D) and/or vaporization (V) of groundwater by high gas and/or heat flow derived from a cooling intrusion is primarily responsible for the observed SP anomalies at Masaya (Lewicki et al. 2003). The magnitude of a given SP anomaly here should be proportional to the sum of the fluxes of positively charged water molecules produced by these processes ($F_t^{H2O} = F_V^{H2O} + F_D^{H2O}$). Scaling exponents suggest that there is a declining increase in SP with a given increase in F_s^{CO2}, until a threshold at log $F_s^{CO2} \approx 2.5\ g\ m^{-2}d^{-1}$ above which SP remains relatively constant with increasing F_s^{CO2}.

Lavas and scoria at the Masaya study site are porous and highly fractured. We observe the highest rates of CO_2 (and steam) degassing along linear trends that correspond to the location/trend of the inferred normal fault (Figure 2). Elevated log F_s^{CO2} values (> 2.5 g m^{-2}d^{-1}) along transects C1-C4 also correlate with fault/fracture locations (Figure 3). These observations indicate distinct gas transport mechanisms, where the highest fluxes are likely associated with advective transport along fractures and the moderate to low fluxes are associated with diffusive transport through the porous matrix. Relative to F_s^{CO2}, positive SP anomalies show little variability over short spatial scales (Figure 3) and do not reflect the presence or absence of fractures. Hence, at elevated F_s^{CO2} values, log SP becomes poorly correlated with log adjusted F_s^{CO2}.

One explanation for the observed scaling relationship between SP and adjusted F_s^{CO2} may be the presence of two sources of CO_2 degassing at depth. Based on carbon isotopic compositions of soil CO_2 at Masaya, this CO_2 is ultimately derived from deep magmatic/marine carbonate sources (Lewicki et al. 2003). However, CO_2 exsolved from the cooling intrusion may either be dissolved in and subsequently degas from the groundwater system due to changes in subsurface temperatures, or rise directly to the surface. In the former case, we would expect a positive (although not necessarily linear) correlation between CO_2 flux and SP, as areas of high heat flow will cause both CO_2 degassing from the groundwater and vaporization of groundwater yielding F_V^{H2O}. The charged water vapor and CO_2 may then rise through the porous medium, creating relatively broad surface anomalies in SP and F_s^{CO2}. In the later case, CO_2 (and steam) degassed from the intrusion may rise directly to the surface along highly permeable fractures

with minimal interaction with groundwater, producing the highest soil gas fluxes. If relatively low F_V^{H2O} is consequently produced during this process, then we would not expect SP to be correlated with F_s^{CO2} over the high F_s^{CO2} range. It is also unlikely that steam exsolved from the high-temperature intrusion would produce an SP anomaly, due to the absence of F_V^{H2O} production at temperatures $> \sim 400^o$C (Blanchard 1964). Therefore, the scaling relationships observed in Figure 4 may be related to two CO_2 flux populations, a low-flux population associated with groundwater degassing/vaporization and positive correlation of SP and F_s^{CO2}, and a high-flux population associated with direct gas flow from depth along fractures and poor SP-F_s^{CO2} correlation.

The scaling relationship observed between SP and adjusted F_s^{CO2} may alternatively be explained by the influence of CO_2 flow on the SP anomaly by fluid disruption. With RFD, we would expect positive correlation between bulk gas flux from depth and SP; however, there may be a non-linear relationship between this gas flux and the number of water molecules ripped from the fluid (F_D^{H2O}). This may explain the scaling relationship between adjusted F_s^{CO2} and SP at adjusted $F_s^{CO2} \leq 2.5\ g\ m^{-2}d^{-1}$. Above this F_s^{CO2} threshold, we observe a plateau in SP with adjusted F_s^{CO2} which may be due to local removal and depletion of the fluid source for RFD from the rock, leading to a plateau in SP versus adjusted F_s^{CO2} flux.

While intriguing trends are observed in SP and F_s^{CO2} data at Masaya, a range of processes may explain these trends. To use concurrent measurements of SP and F_s^{CO2} to better understand processes operating at depth in the volcanic system, additional field, laboratory, and numerical experiments are required to define the relationships between these parameters under a range of hydrogeologic and fluid/heat source conditions.

REFERENCES

Anderson, L. A. and G. R. Johnson (1976). Application of the self-potential method to geothermal exploration in Long Valley, California. *J. Geophys. Res. 81*, 1527–1532.

Babu, R. (2003). Relationship of gravity, magnetic, and self-potential anomalies and their application to mineral exploration. *Geophysics 68*, 181–184.

Blanchard, D. C. (1964). Charge separation from saline drops on hot surfaces. *Nature 201*, 1164–1166.

Corwin, R. F. and D. B. Hoover (1979). The self-potential method in geothermal exploration. *Geophysics 44*, 226–245.

Fitterman, D. V. and R. F. Corwin (1982). Inversion of self-potential data from the Cerro-Prieto geothermal field, Mexico. *Geophysics 47*, 938–945.

Hashimoto, T. and Y. Tanaka (1995). A large self-potential anomaly on Unzen volcano, Shimabara peninsula, Kyushu island, Japan. *Geophys. Res. Lett. 22*, 191–194.

Ishido, T. and J. W. Pritchett (1999). Numerical simulation of electrokinetic potentials associated with subsurface fluid flow. *J. Geophys. Res. 104*, 15,247–15,259.

Johnston, M. J. S., J. D. Byerlee, and D. Lockner (2001). Rapid fluid disruption: A source for self-potential anomalies on volcanoes. *J. Geophys. Res. 106*, 4327–4335.

Lewicki, J. L., C. Connor, K. St-Amand, J. Stix, and W. Spinner (2003). Self-potential, soil co_2 flux, and temperature on Masaya volcano, Nicaragua. *Geophys. Res. Lett. 30*, 1817.

Massenet, F. and V. N. Pham (1985). Mapping and surveillance of active fissure zones on a volcano by the self-potential method, Etna, Sicily. *J. Volcanol. Geotherm. Res. 24*, 315–338.

Revil, A., H. Schwaeger, L. M. C. III, and P. D. Manhardt (1999). Streaming potential in porous media 2. Theory and application to geothermal systems. *J. Geophys. Res. 104*, 20,033–20,048.

Zlotnicki, J., Y. Sasai, P. Yvetot, Y. Nishida, M. Uyeshima, F. Fauquet, H. Utada, Y. Takahashi, and G. Donnadieu (2003). Resistivity and self-potential changes associated with volcanic activity: The July 8, 2000 Miyake-jima eruption (Japan). *Earth Planet. Sci. Lett. 205*, 139–154.